The Impact of Giant Cloud Condensation Nuclei on Drizzle Formation in Stratocumulus: Implications for Cloud Radiative Properties

GRAHAM FEINGOLD

Cooperative Institute for Research in the Atmosphere/NOAA, Environmental Technology Laboratory, Boulder, Colorado

WILLIAM R. COTTON, SONIA M. KREIDENWEIS, AND JANEL T. DAVIS

Department of Atmospheric Science, Colorado State University, Fort Collins, Colorado

(Manuscript received 4 May 1998, in final form 4 January 1999)

ABSTRACT

The impact of giant and ultragiant cloud condensation nuclei (>5-μm radius) on drizzle formation in stratocumuli is investigated within a number of modeling frameworks. These include a simple box model of collection, a trajectory ensemble model (comprising an ensemble of Lagrangian parcel models), a 2D eddy-resolving model, and a 3D large-eddy simulation model. Observed concentrations of giant cloud condensation nuclei (GCCN) over the ocean at ambient conditions indicate that 20-μm radius haze particles exist in concentrations of between 10^{-4} and 10^{-2} cm^{-3}, depending on ambient wind speed and seastate. It is shown that these concentrations are sufficient to move a nonprecipitating stratocumulus into a precipitating state at typical cloud condensation nucleus (CCN) concentrations of 50 to 250 cm^{-3}, with higher concentrations of GCCN being required at higher CCN concentrations. However, at lower CCN concentrations, drizzle is often active anyway and the addition of GCCN has little impact. At high CCN concentrations, drizzle development is slow and GCCN have the greatest potential for enhancing the collection process. Thus, although drizzle production *decreases* with increasing CCN concentration, the relative impact of GCCN *increases* with increasing CCN concentration. It is also shown that in the absence of GCCN, a shift in the modal radius of the CCN distribution to larger sizes suppresses drizzle because larger modal radii enable the activation of larger droplet number concentrations. Finally, calculations of the impact of GCCN on cloud optical properties are performed over a range of parameter space. Results indicate that the presence of GCCN moderates the effect of CCN on optical properties quite significantly. In the absence of GCCN, an increase in CCN from 50 to 150 cm^{-3} results in a threefold increase in albedo; when GCCN exist at a concentration of 10^{-3} cm^{-3}, the increase in albedo is only twofold. Thus the variable presence of GCCN represents yet another uncertainty in estimating the influence of anthropogenic activity on climate.

1. Introduction

The role of giant cloud condensation nuclei (GCCN), loosely defined here as cloud condensation nuclei (CCN) with radii greater than 5 μm, has been a matter of much speculation in the field of cloud and precipitation microphysics. Houghton (1938) put forward the notion that GCCN could modify the colloidal stability of a cloud of droplets by generating droplets with sizes large enough that they could collect the ambient cloud droplets through collision and coalescence. Measurements of the concentration of sea-salt particles emitted from an ocean surface (Woodcock 1953) were valuable in establishing the concentrations of GCCN as a function of wind speed. One of the major problems with these measurements is that they were made at some fixed relative humidity (RH), somewhat less than ambient, so that assumptions about particle size at ambient, subcloud conditions have to be made to derive the concentration of particles at any given size. This problem is more pernicious than one might imagine; although RH profiles provide necessary information for calculating the size of haze particles, the time required for particles to achieve equilibrium with their environment is a rapidly increasing function of particle size. Thus, while one might assume equilibrium sizes for small particles (<about 0.1-μm radius; Mordy 1959), based on Köhler curve calculations for known particle chemistry and RH to reasonable accuracy, one cannot make such an assumption for larger particles who may take many hours to reach equilibrium. Given that the eddy turnover time in the boundary layer (BL) scales as the BL depth divided by the convective velocity scale (which is typically about 10 or 15 min), some information would be

Corresponding author address: Graham Feingold, CIRA/NOAA Environmental Technology Laboratory, 325 Broadway, Boulder, CO 80303.
E-mail: gfeingold@etl.noaa.gov

required on the extent of BL mixing, the trajectory history of particles, and possible sojourns into cloud during the preceding period, before one could attempt to infer the sizes of GCCN under ambient conditions.

To circumvent these difficulties, others (e.g., Exton et al. 1986; Kim et al. 1995) have measured haze particles under ambient subcloud conditions with the aid of airborne spectrometers (Forward Scattering Spectrometer Probe or FSSP; Particle Measuring Systems Inc.). The FSSP is designed to sample particles in the radius range $1 < r < 25$ μm. It is currently accepted that drops with $r > 19$ μm have significant collection efficiencies when interacting with smaller cloud droplets, and have the potential to initiate precipitation-sized drops (e.g., Klett and Davis 1973). Although there is continued interest in the effects of turbulence on the collection kernels (e.g., Saffman and Turner 1956; Khain and Pinsky 1995), these have yet to be satisfactorily resolved. Considering then the widely accepted 19-μm threshold, the largest particles sampled by the FSSP are of greatest interest since they have the potential to form drops of at least this radius, and interact with other cloud droplets, *regardless of whether they (the GCCN) are considered activated droplets according to Köhler theory* (e.g., Johnson 1982).

Giant CCN have implications for the precipitation process, as indicated by works that have considered the role of naturally occurring giant and ultragiant ($r > 10$ μm) particles in rain formation via collection (Johnson 1982), as well as via the hygroscopic seeding process to augment rainfall in warm-phase clouds (e.g., Tzivion et al. 1994; Cooper et al. 1997). Using measured CCN spectra as input to a parcel model, Johnson (1982) showed that the concentrations of naturally occurring GCCN are sufficient to initiate collection, even in colloidally stable clouds, although the results did indicate that the more stable the cloud, the more important the existence of GCCN for effective rain formation. Levin et al. (1996) proposed that giant dust particles coated with sulfate could be effective enhancers of precipitation. Tzivion et al. (1994) examined hygroscopic seeding within the framework of a 2D axisymmetric cloud model and stressed the importance of time and location of seeding for most effective results. Cooper et al. (1997) used a Lagrangian parcel model to study the seeding process. A high-resolution, fixed-bin collection model was coupled with a moving-grid model of droplet condensation to eliminate numerical diffusion and spurious spectral broadening. Results indicated that hygroscopic seeding is expected to yield precipitation augmentation in the clouds studied. Unfortunately, experimental verification of these modeling studies is nontrivial.

Stratocumuli produce only modest amounts of precipitation at the surface, so the impact of GCCN is of interest for reasons other than precipitation or its augmentation. One role of drizzle in stratocumuli that has received recent attention is its effect on BL dynamics through the vertical redistribution of heat and vapor (Paluch and Lenschow 1991; Feingold et al. 1996a; Stevens et al. 1998b). Another aspect of the role of GCCN, and the focus of this paper, is their impact on cloud optical properties. Stratocumuli have been identified as having a potentially significant impact on climate because they modify the earth's shortwave albedo compared with the underlying ocean, but radiate in the longwave at approximately the same temperature as the surface. Moreover, they occur with high frequency and have extensive spatial coverage (annually averaged cloud cover is 34%) (Warren et al. 1986). The radiative impact of clouds is closely related to their optical depth and albedo, which are strong functions of droplet size (Stephens 1978) and albedo susceptibility, defined as the change in albedo for a unit increase in drop concentration (Twomey 1991). The addition of small concentrations of GCCN will have negligible *direct* impact on drop concentration, albedo, optical depth, or susceptibility; however, if they can initiate the drizzle process their impact can be considerable. The most straightforward avenue for this is through depletion in cloud water, although broadening of the drop size spectrum has also been shown to be important (Feingold et al. 1997). However, the intimate coupling between microphysics and boundary layer dynamics is such that feedback to the dynamics may be significant (Stevens et al. 1998b) with possible changes to the convective nature of the BL, cloud cover, cloud depth, and ability of clouds to precipitate in subsequent cycles.

This paper, therefore, follows similar works (particularly that of Johnson 1982) in its attempt to evaluate the impact of GCCN on collection, but differs in that it (i) addresses the impact on cloud optical properties and BL dynamics as well as on precipitation, and (ii) employs a range of numerical models including a powerful, large-eddy simulation model in order to address these issues. The goal is to explore scenarios under which ambient GCCN in the marine BLs are expected to have an impact on optical properties and BL dynamics.

2. Measurements of GCCN

Some early measurements of GCCN emitted by the ocean surface were not performed at ambient conditions; therefore assumptions about RH need to be invoked when building size spectra. In this work we avail ourselves of measurements performed during the First Aerosol Characterization Experiment (ACE-1) over the Southern Ocean in 1995. Haze particle spectra at ambient conditions were compiled from an airborne FSSP. Data were sorted into two broad RH bands: $85 \leq \text{RH} < 95\%$, and $75 \leq \text{RH} < 85\%$. In both cases, significant variability existed and indicated concentrations of haze particles in the largest FSSP bin (centered at $r = 23$ μm, with a bin width of 7 μm) of between 10^{-4} and 10^{-2} cm^{-3}, with no clear dependence on the RH regime. These particles are most likely sea-salt particles with

dry radii on the order of 6 to 12 μm (assuming complete solubility and equilibrium sizes between 75% and 95% RH). Their critical radii would be on the order of millimeters, so that they clearly would participate in droplet interactions as haze particles rather than as activated drops.

These observations are similar to other measurements using FSSP probes and optical array probes; for example, surface measurements over the northeast Atlantic by Exton et al. (1986) indicate total particle concentrations in the range $1 < r < 23.5$ μm of a few-per-centimeter cubed, and in the range $5 < r < 150$ μm, of about 0.1–0.5 cm^{-3}. Their rather high concentrations of particles at about 25-μm radius suggest that jet-droplet production from breaking waves is the dominant production mechanism (Blanchard 1982). Exton et al.'s airborne measurements indicated a 25% loss in particle concentration at 30 m above the surface, and further losses are expected higher up in the boundary layer when mixing is inefficient.

The variability in GCCN concentrations is large, be it due to changes in sea state or poor mixing of large particles to cloud altitude, and for this reason the GCCN concentrations used in these numerical experiments will be varied over a similar range. In addition, the variability in the CCN spectra that is evident in measurements suggests that use of parametrized CCN spectra is warranted. Thus, rather than use any given measured spectrum as input to the model, CCN spectra will be represented by lognormal functions, whose parameters are varied to reflect natural variability.

3. Results

a. Multiple modeling frameworks

The results to be presented here emanate from a hierarchy of models, each exhibiting an increase in the complexity of the physics. The box model of collection assumes a closed box and constant liquid water content and is useful for estimating timescales for collection for a very broad range of phase space. The more complex trajectory ensemble model (described below) improves upon the box model by representing the temporal–spatial variability in cloud water content, albeit over a more limited part of phase space. It enables a clear picture of the effect of GCCN on the microphysics and a separation of these issues from feedbacks to the dynamics. Finally, the dynamical–microphysical model represent even more complexity by investigating the fully coupled system. However it is limited to a much smaller region of phase space.

This hierarchy of models has been applied in an effort to facilitate understanding of the CCN–cloud system. In addition, because models are virtually impossible to verify, the emergence of a robust feature from different modeling frameworks provides greater confidence in the result. If a result emerges from one model only, one must question its validity, especially if it is derived from a simple system. A result that emerges from the most complex model may be more valid than the others, yet it does not necessarily represent the most effective means of understanding the system. Also, because it includes so much complexity it relies on more parameterizations of physical processes and is therefore more susceptible to error. For these reasons it behooves us to apply a variety of models for a reasonable number of scenarios before challenging the observationalists to explore the ideas presented in this paper.

b. Box model of collection

The stochastic collection model of Tzivion et al. (1987) is used to represent collection, regardless of the modeling framework. The solution is based on a multimoment approach that conserves cloud water by design and also solves for drop concentration. It resolves the drop size distribution into 25 size bins covering the range 1.5 to 500 μm in 25 size bins (with mass doubling from one bin to the next). Within in each bin, equations for both drop mass and number concentration are solved. Comparison of the numerical solution with analytical solutions for simple kernels shows excellent agreement and negligible anomalous spreading. The collection kernel compiled by Hall (1980) is used to characterize drop interactions. Using this collection model, we can map out some parameter space in a box-model framework and evaluate the timescales required for drizzle formation under typical stratocumulus conditions.

The initial conditions for this model are drop number N_0, liquid water content (LWC), and an assumed drop dispersion. Initial spectra are assumed to be lognormal with a geometric standard deviation σ_g of 1.2 (relative dispersion of 0.18). Use of different values of σ_g changes the results in a quantitative sense, but the main ideas are robust. The LWC is varied over the interval (0.15 g m^{-3}; 1.1 g m^{-3}), and N_0 is varied over the range (10 cm^{-3}; 1000 cm^{-3}). When simulating the effects of GCCN on the collection process, it is assumed that they produce drops of radius 20 μm. Figures 1a and b show contour plots of the time required for 10% of the cloud water to be transferred to drizzle water (defined here as drops with radius $r > 20$ μm) in N_0, LWC space, both with and without GCCN at concentrations of 10^{-3} cm^{-3}. At high LWC and low N_0, collection is rapid enough that the GCCN do not affect the results at all; the difference in time for 10% of the cloud water to be transferred to drizzle water for N_0 on the order of 50 cm^{-3} is $<$1% for LWC $>$0.3 g m^{-3} (Fig. 1c). For LWC $=$ 0.6 g m^{-3} and $N_0 = 200$ cm^{-3}, GCCN at the 10^{-3} cm^{-3} level decreases the time required for 10% of the cloud water to be transferred to drizzle water from 55 to 46 min, or about 16%. Finally, at low LWC and high N_0, the time required exceeds 120 min and has therefore not been plotted.

When evaluating these effects, it is important to consider that the typical parcel in-cloud residence times are on the order of 20 min for well-mixed marine boundary

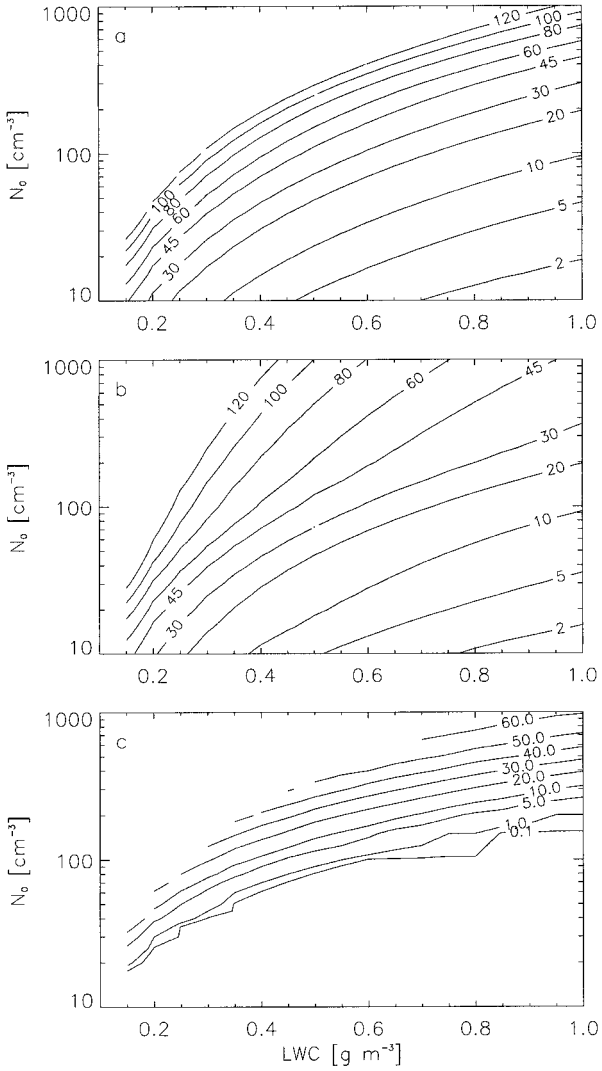

FIG. 1. Contours of the time (min) required for 10% of the LWC to be transferred to drizzle (drops with $r > 20$ μm) through the collection process as a function of initial drop number N_0 and LWC, (a) no GCCN, (b) 10^{-3} GCCN cm^{-3}, (c) percentage difference between (a) and (b).

layers, with only a small fraction of parcels spending 60 min in cloud (Stevens et al. 1996; Feingold et al. 1998). The details of the probability density function (PDF) of in-cloud residence time do vary from one BL to another and need to be considered on a case-by-case basis. Thus, the potential for influence of GCCN is rather restricted, and most likely resides in the area beneath the 60 min contour level in Fig. 1a or 1b. For BLs with N_0 on the order of 150 cm^{-3}, this region is limited to LWC >about 0.45 g m^{-3}.

c. Trajectory ensemble model

Using results such as those in Fig. 1, one might attempt to evaluate the overall effect of GCCN on collection by weighting the magnitude of the GCCN effect on drizzle with the frequency of occurrence of a given parcel in-cloud residence time (see Feingold et al. 1996b):

$$\overline{D} = \frac{\int f(t)d(t)\,dt}{\int f(t)\,dt}, \tag{1}$$

where $f(t)$ is the PDF of in-cloud residence time, $d(t)$ represents the drizzle production rate, and $\overline{D}$ the mean drizzle production rate for an ensemble of parcel trajectories. However, the collection process is very sensitive to LWC and the mean LWC is a poor surrogate when LWC is fluctuating (Twomey 1976). Thus it is important to represent the spatial and temporal fluctuations in LWC if one is to address this problem more rigorously. Following Stevens et al. (1996) and Feingold et al. (1998) we apply the trajectory ensemble model (TEM) framework. This approach derives an ensemble of trajectories from a large-eddy simulation (LES, see below) and uses these trajectories to drive a set of 500 parcel models with size-resolved aerosol and cloud microphysics. The main advantages and disadvantages of this approach have been discussed in detail in the aforementioned references but are briefly adumbrated here. Because the trajectories are derived from the LES, they represent 3D dynamics. The TEM is useful for isolating microphysical processes because no feedback to the dynamics is allowed. By running a multitude of parcels—each having its own thermodynamic and kinematic properties, in-cloud residence time, and liquid water content history—and then averaging the results, one obtains a much more representative picture than would be obtained from a boxmodel or from a single parcel run. The main drawback of this approach is that all drops are assumed to follow parcel trajectories; thus, it does not represent drop sedimentation and precipitation (see also Cooper et al. 1997). In addition, interparcel mixing is not represented on timescales less than 1 h and this limits the applicability of the results. Nevertheless, the goal in this section is to examine the combined condensation-collection growth with and without the presence of giant CCN *in a framework that allows for realistic spatial–temporal fluctuations in LWC.* In the subsequent section Eulerian models will be used to represent all processes, including precipitation.

1) MODEL PHYSICS

Each parcel in the TEM uses a bin microphysical representation of the drop spectrum. Droplet activation, condensation–evaporation, and collection are solved using moment-conserving techniques as described in Tzivion et al. (1987) and Stevens et al. (1996). Following droplet activation, particles are tracked as solute in the

drop spectrum, and regenerated to particles on complete evaporation (Feingold et al. 1996b). In all cases great care has been taken to reduce the numerical diffusion that would produce unrealistic time scales for the production of large drops. The activation scheme is as described in Feingold et al. (1996b) with some modifications. The CCN spectrum is represented by 14 logarithmically broadening size bins ranging from 0.015 to 6 μm radius. The CCN are assumed to be ammonium sulfate, except for the largest bin which is sodium chloride. Small aerosol particles (<1 μm) are assumed to form droplets between 1.5 and 2 μm, whereas particles >1 μm are mapped to drop bins assuming 97% RH equilibrium sizes, in approximate agreement with Mordy (1959). For the initial conditions considered in these experiments, all CCN form droplets between 1.5 and 2 μm, and the only large drops formed are due to GCCN in the largest size bin. These are assumed to form droplets of 20-μm radius. As discussed in section 2, concentrations of GCCN are inferred from measurements of haze particles under ambient conditions so that no assumptions need be made about the size of the nucleus on which the haze particle formed, nor about its history prior to entering the cloud. We have limited our discussion to haze particles with radii of 20 μm. Haze particles of smaller sizes (on the order of 10 μm) will shorten the time required to produce 20-μm drops (e.g., Cooper et al. 1997) but, given that the current treatment of activation is a parameterization of the real process, we do not feel it appropriate to add complexity that is not well resolved by the model.

2) LES SIMULATION AS A SOURCE OF PARCEL TRAJECTORIES

The LES model is used to simulate the ''First Lagrangian Experiment'' associated with the Atlantic Stratocumulus Transition Experiment (ASTEX) (Albrecht et al. 1995). The case has been well documented with observations (Bretherton et al. 1995) and numerical simulations (Wyant et al. 1997; Stevens et al. 1998b). Initial soundings are taken from the GEWEX Cloud System Studies (GCSS) workshop case study (Duynkerke et al. 1995) and are described more fully in Stevens et al. (1998b). In order to generate a set of trajectories, the LES is first spun up to the point where turbulence is fully developed; then, at 100 min after model initialization, 500 parcels are tagged below the cloud. These parcels are then tracked for 1 h, and their positions, velocities, and thermodynamic properties are recorded. The 500 trajectories are later used to drive 500 individual parcel models.

For the first experiment, CCN spectra are assumed to conform to a lognormal size distribution with total number concentration $N_{\rm ccn} = 50$ cm^{-3}, median radius $r_g = 0.1$ μm, and geometric standard deviation $\sigma_g = 1.8$. Figure 2 shows sample profiles of water mixing ratio and drop number, averaged over the 1-h period for four different simulations. In creating the profiles, contributions to the variable are sorted into 10-m height bins. The first simulation assumes no collection; the second enables collection; the third is the same as the second except that 10^{-3} cm^{-3} GCCN are ''seeded'' [1] in the CCN spectrum; and finally, the fourth seeds the CCN spectrum with 10^{-2} cm^{-3} GCCN. The left panel indicates drop water mixing ratio r_l for cloud droplets ($r < 20$ μm) and drizzle drops ($r > 20$ μm),[2] and the right panel indicates drop number concentrations N in these same size categories. To facilitate comparison of the relative amounts of cloud and drizzle, logarithmic scales have been used for the abscissae. (On a linear plot, r_l shows the characteristic linear profile expected in stratocumuli.) For these low $N_{\rm ccn}$, tiny amounts of drizzle water are produced through condensation alone (see also Johnson 1982; maritime case) but when collection is enabled, drizzle water is far more prevalent, especially near cloud top. Note that although drizzle-sized drops are produced primarily at cloud top where r_l is highest, they can be mixed down through the cloud by the parcels due to the assumption that droplets follow parcel trajectories. Seeding of GCCN at the 10^{-3} cm^{-3} level produces almost no enhancement in drizzle production, whereas for concentrations of 10^{-2} cm^{-3}, significantly more drizzle is produced and appears through a greater depth of the cloud. Table 1 summarizes the impact of collection and GCCN on the path-integrated drizzle amount in g m^{-2} [i.e., the liquid water path (LWP) contained in drops >20 μm]. By itself, collection transfers 25% of the LWP to drizzle drops, and GCCN at 10^{-3} cm^{-3} hardly changes this. Adding GCCN at 10^{-2} cm^{-3} increases this by a modest amount to 31.8% (a relative increase of 28%).

Simulations are repeated for $N_{\rm ccn} = 150$ cm^{-3} (Fig. 3) where it is apparent that in the absence of collection, no drizzle drops are produced. The collection process initiates appreciable amounts of drizzle water near cloud top, although somewhat less compared to $N_{\rm ccn} = 50$ cm^{-3}, due to greater competition among drops for available vapor. A GCCN concentration of 10^{-3} cm^{-3} produces a noticeable effect on drizzle formation, and this is enhanced even further at 10^{-2} cm^{-3}. The relative increase in drizzle LWP due to GCCN is much greater than for $N_{\rm ccn} = 50$ cm^{-3} (Table 1).

Again, simulations are repeated, but this time for $N_{\rm ccn} = 250$ cm^{-3} (Fig. 4), resulting in even lower amounts of drizzle. In the absence of GCCN, collection produces drizzle only in the region right at cloud top; adding GCCN extends this region down through more of the

[1] The term ''seeding'' is used to imply the insertion of GCCN into the CCN spectrum, rather than in the sense of seeding associated with rainfall enhancement.

[2] We use r_l [g kg^{-1}] rather than LWC [g m^{-3}] because r_l is conservative for vertical motions; in-cloud air density is on the order of 1.15×10^{-3} so that LWC $\approx r_l \times 1.15$; deviations over the depth of the cloud are negligible.

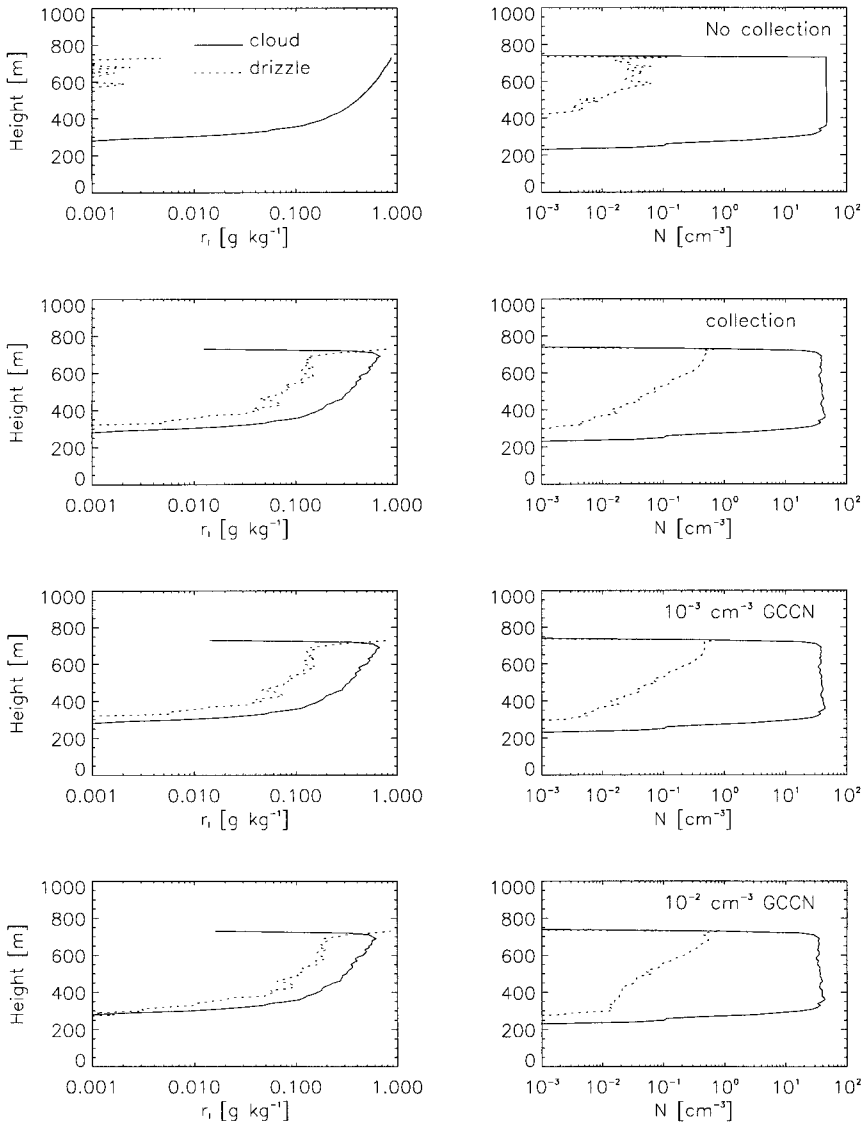

FIG. 2. Hourly averaged profiles of water mixing ratio r_l (left panel) and drop number N (right panel) generated by the TEM for cases without collection, with collection, with 10^{-3} GCCN cm^{-3}, and with 10^{-2} GCCN cm^{-3}. Solid lines indicate cloud water mixing ratio or number concentration; dashed lines indicate drizzle water mixing ratio or number concentration. The CCN spectrum is defined by $N_{ccn} = 50$ cm^{-3} and $r_g = 0.1$ μm.

TABLE 1. Percentage of LWP contained in drizzle drops for TEM simulations. Cases include: no collection, collection, GCCN at 10^{-3} cm^{-3}, and GCCN 10^{-2} cm^{-3} for initial CCN concentrations of 50, 150, and 250 cm^{-3}.

	N_{ccn} [cm^{-3}]		
	50	150	250
No collection	0.15	0.00	0.00
Collection	24.9	1.70	0.04
10^{-3} GCCN	25.7	3.90	1.72
10^{-2} GCCN	31.8	14.0	7.90

cloud. Although drizzle amounts become progressively smaller with increasing N_{ccn}, the relative impact of GCCN becomes progressively stronger (Table 1).

In Fig. 5, the range of GCCN concentrations is extended and drizzle-water mixing ratio r_d is plotted as a function of GCCN amount and N_{ccn}. The results show quite clearly that the impact of GCCN is felt mostly at large N_{ccn} where the potential exists to increase r_d by about one-and-a-half orders of magnitude. Nevertheless, it is stressed that the absolute amounts of drizzle that develop when GCCN exist at concentrations of 10^{-2} cm^{-3} and N_{ccn} is 150 cm^{-3}, are significantly less than when $N_{ccn} = 50$ cm^{-3} and GCCN are absent.

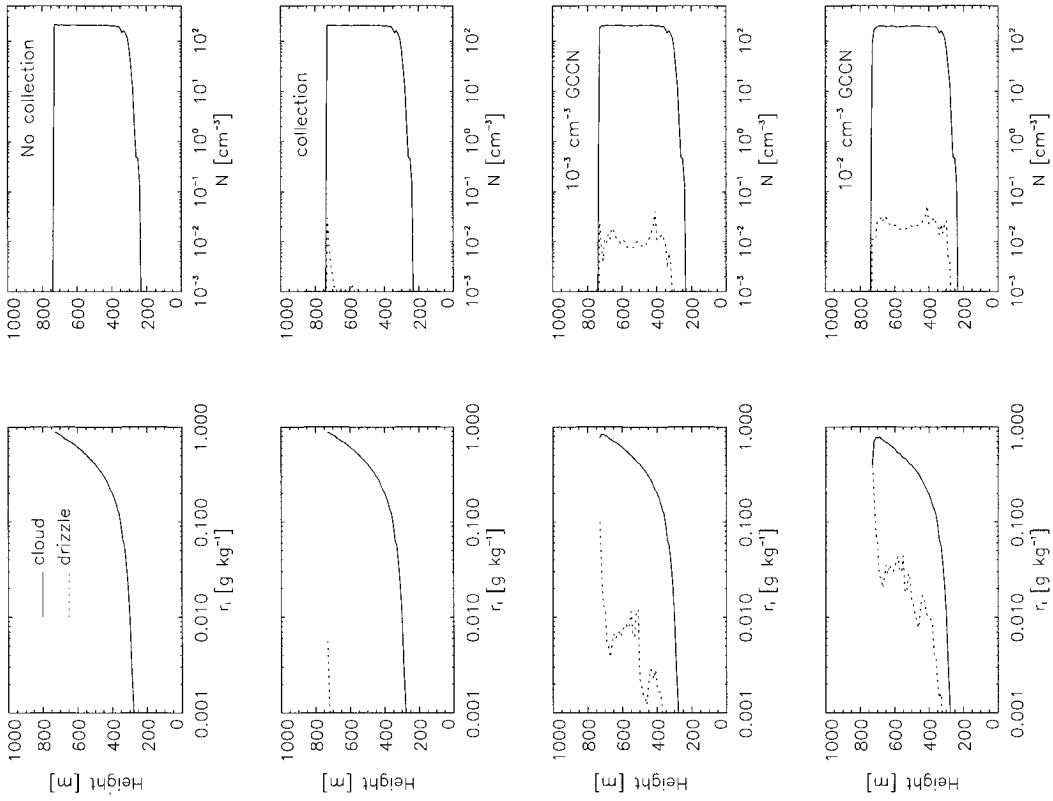

FIG. 4. As in Fig. 2 but for a CCN spectrum defined by $N_{ccn} = 250$ cm^{-3} and $r_g = 0.1$ μm.

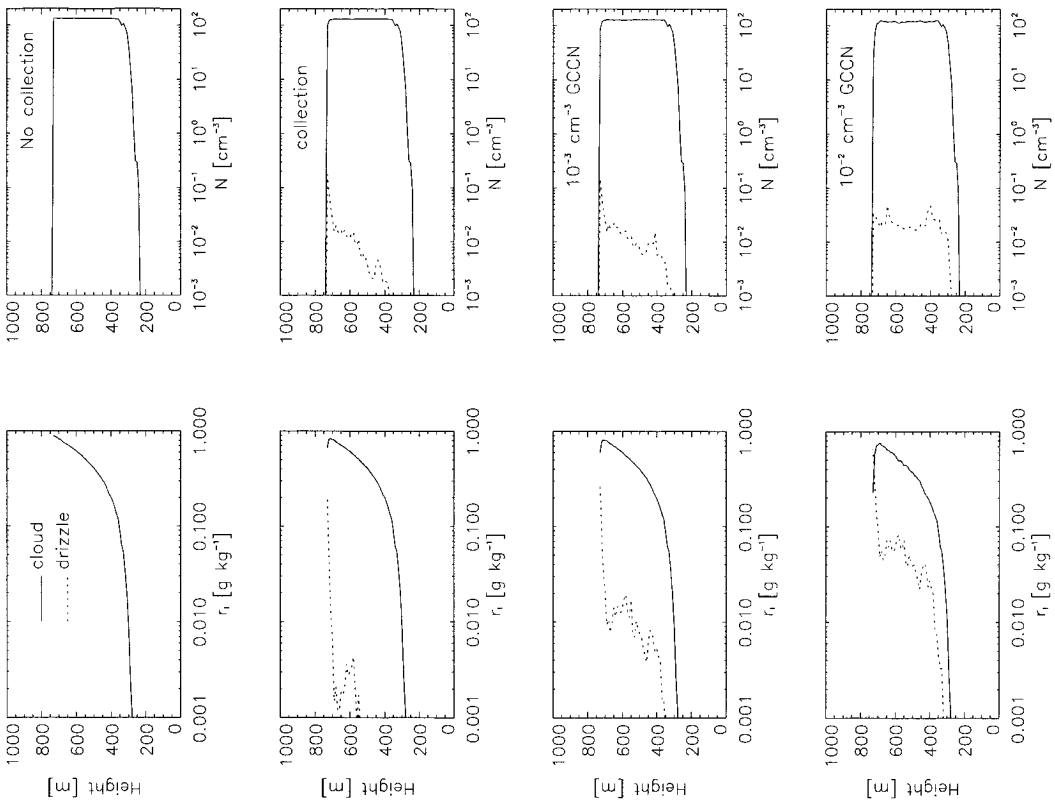

FIG. 3. As in Fig. 2 but for a CCN spectrum defined by $N_{ccn} = 150$ cm^{-3} and $r_g = 0.1$ μm.

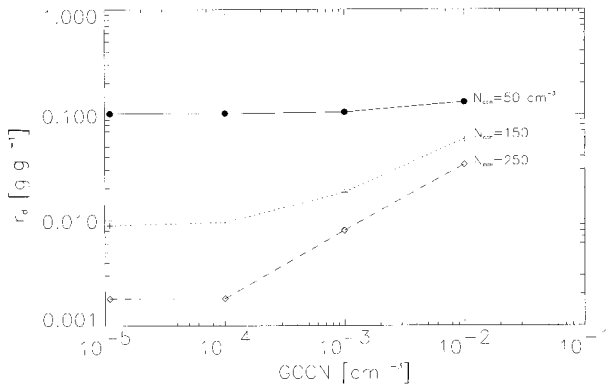

FIG. 5. Drizzle water content r_d as a function of GCCN concentration for the simulations in Figs. 2–4.

A number of selected TEM simulations are now performed for a CCN spectrum having $r_g = 0.05$ μm, and then compared with those for which $r_g = 0.1$ μm (Fig. 6a). It is noted that for all N_{ccn}, runs with $r_g = 0.05$ μm produce more drizzle than those for which $r_g = 0.1$ μm. However, when the spectrum with $r_g = 0.1$ includes 10^{-2} cm^{-3} GCCN, more drizzle is produced than when $r_g = 0.05$ μm and no GCCN are present. The smaller r_g results in fewer droplets activated, less competition for growth, and, because LWC is essentially the same (only very small amounts of r_l reside in supersaturation), droplets are commensurately larger. Figure 6b indicates that the percentage difference in drizzle water r_d due to GCCN increases steadily with increasing N_{ccn}, and that at $N_{ccn} = 150$ cm^{-3}, this difference is significantly less for $r_g = 0.05$ μm than it is for $r_g = 0.1$ μm. As in Fig. 5, the explanation is that for $r_g = 0.05$ μm the drizzle process is already significantly stronger than it is for $r_g = 0.1$ μm, so that GCCN at this concentration have less impact. Also shown in Fig. 6b is the percentage difference in r_d resulting from the shift in r_g from 0.1 to 0.05 μm, as a function of N_{ccn}. It is seen that at $N_{ccn} = 150$ cm^{-3}, this enhancement in drizzle is maximal which suggests that a shift in median particle size causes a different qualitative response in drizzle formation than does the inclusion of GCCN. To the extent that these results are true to natural drizzle processes, they indicate a rather complex response of the system to both size and number concentration of CCN, as well as to number concentration of GCCN (the size of GCCN is not varied in these experiments).

d. Eddy-resolving model and large-eddy simulation model

Further simulations are now performed with the coupled dynamical–microphysical eddy-resolving model (ERM), and the LES described in detail by Feingold et al. (1996a,b) and Stevens et al. (1996), respectively. These models are identical except that the ERM is two-dimensional whereas the LES is three-dimensional.

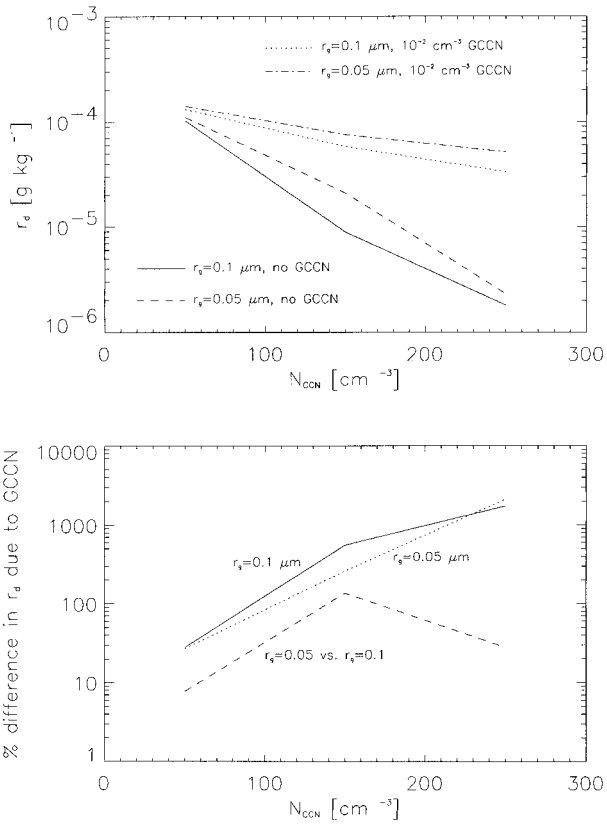

FIG. 6. (a) Drizzle water content r_d [g kg^{-1}] as a function of CCN concentration for various CCN spectra, and GCCN concentrations; (b) percentage difference in r_d caused by the addition of GCCN (for a given median particle radius, r_g), or due to the change in median particle radius.

Were it feasible, all coupled simulations would have been performed in the LES framework since it provides our best representation of BL eddy structure. However, the computational expense of LES would have severely restricted the number of model integrations and it was deemed more pragmatic to perform these simulations in the 2D ERM and cover more scenarios. This is especially true of the current simulations which resolve both CCN and drop size distributions, necessitating prognostic equations for over 100 scalars. The 2D ERM attempts to represent 3D turbulence in only two dimensions and therefore the results it produces must be viewed with caution. However, it does at least include the essential interactions between large eddies and cloud microphysical properties (for a critical review see Stevens et al. 1998a) and therefore provides a valuable framework for testing hypotheses without excessive computational expense.

The ERM–LES models are coupled to the microphysical model described above. In this framework, cloud microphysical processes can respond to spatially and temporally resolved eddies, with full coupling between microphysics and dynamics, including the effects of explicitly resolved advection and subgrid-scale eddy

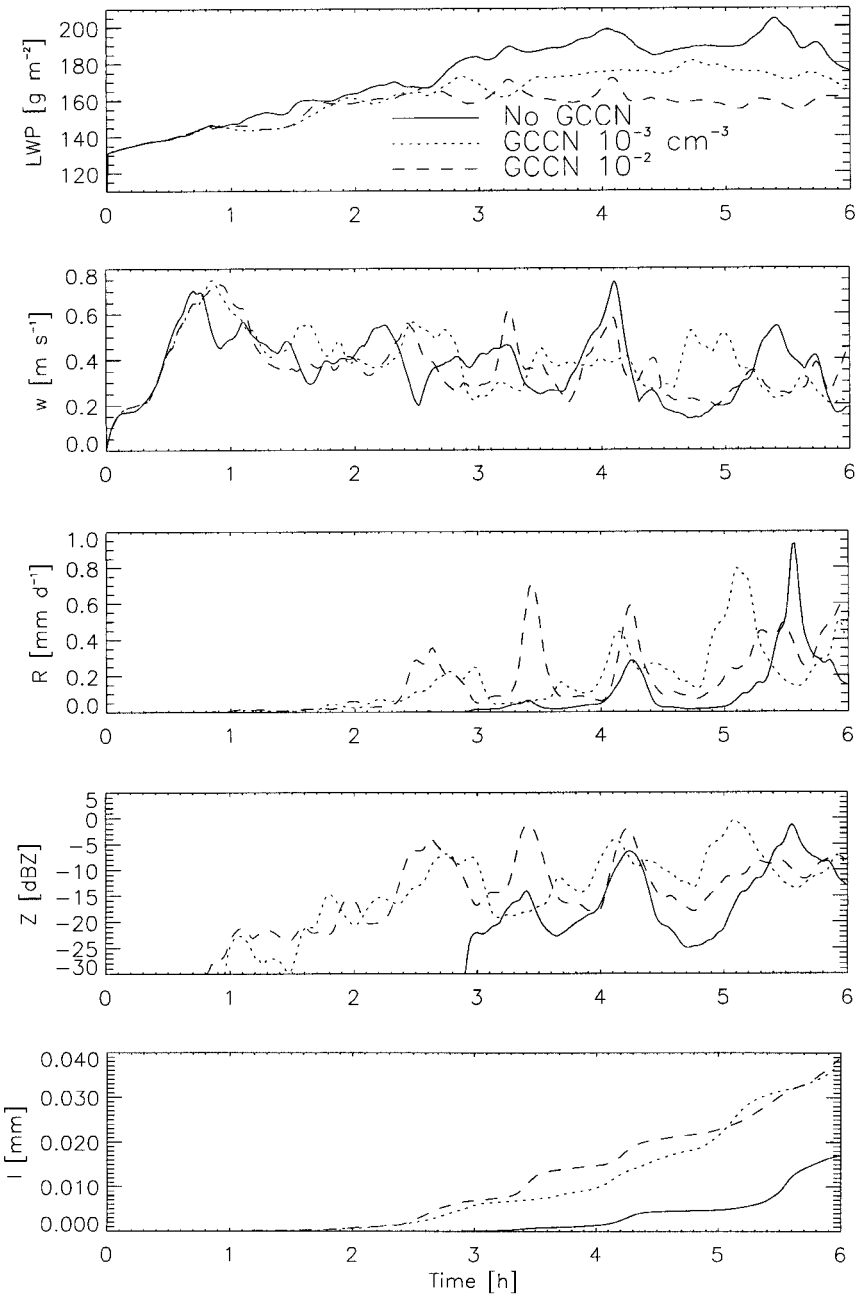

FIG. 7. Time series of domain-averaged quantities obtained from ERM simulations. The CCN spectrum is given by $N_{ccn} = 150$ cm^{-3} and $r_g = 0.1$ μm. Simulations are for cases with no GCCN, and for cases where various concentrations of GCCN have been added: (a) LWP, (b) w_{rms}, (c) surface drizzle rate R, (d) surface drizzle reflectivity Z, and (e) integrated surface precipitation.

diffusion. By simulating sedimentation, these models allow for a more natural representation of the drizzle process than is afforded by the TEM.

1) ERM: $N = 150$ cm^{-3}, $r_g = 0.1$ μm

The model is initialized with the aforementioned ASTEX Lagrangian 1 sounding and a lognormal CCN spectrum defined by $N = 150$ cm^{-3}, $r_g = 0.1$ μm, and $\sigma_g = 1.8$. Three 6-h simulations are performed. The first has no GCCN, the second includes 10^{-3} GCCN cm^{-3}, and the third, 10^{-2} GCCN cm^{-3}. All other conditions are identical. Figure 7 shows a time series of a number of fields for the three simulations. These include LWP, root-mean-square vertical velocity w_{rms}, rainrate R, radar reflectivity Z, and integrated rain amount I. The inclusion of GCCN decreases the 6-h average LWP by 6% to 10%, depending on the GCCN concentration. Over

the last 3 h of the simulation the differences in the mean LWP are 9% to 16%. Decreases in the mean $w_{\rm rms}$ over the last 3 h due to GCCN are about 10% for both of the seeded cases and illustrate that even in small concentrations, these large particles have a significant impact on BL dynamics through their effect on drizzle. GCCN cause surface precipitation to appear an hour earlier (Fig. 7c), and first radar signals (associated with the surface precipitation), at the −30 dBZ level, to appear 2 h earlier (Fig. 7d). Maximum rainrates are about 1 mm d^{-1} rather than the typical mm h^{-1} associated with shallow convective rain. Figure 7e compares the time-integrated rain amounts for the three simulations and indicates an increase of over 100% for both runs, but interestingly enough there is no difference between the two seeded cases after 6 h, despite the time-averaged differences in LWP.

2) ERM: $N = 150$ cm^{-3}, $r_g = 0.05$ μm

Two more simulations are performed but this time the median particle size is decreased to 0.05 μm. One run has no GCCN and the other is seeded with 10^{-3} GCCN cm^{-3}. Figure 8 compares the same fields examined in Fig. 7; seeding decreases LWP by 7% (average over the last 3 h) and $w_{\rm rms}$ by 22%. This strong decrease in $w_{\rm rms}$ due to GCCN is noteworthy and is more closely related to the absolute amount, rather than to the relative increase in the amount of precipitation.

Surface drizzle rainrates are significantly higher in the seeded case and peak at 1.6 mm d^{-1}; again, detectable Z at the surface precedes that of the unseeded case by about 1.5 h. Integrated precipitation is significantly higher for both unseeded and seeded cases compared to Fig. 7. A comparison of Figs. 8e and 7e shows that shifting r_g to 0.05 μm has about the same effect on I as including GCCN when $r_g = 0.1$ μm, that is, a doubling of I. The increase in I due to GCCN when $r_g = 0.05$ μm is about 50%. These responses are different in magnitude from those observed in the TEM for similar input (Fig. 6). There, the presence of GCCN when $r_g = 0.1$ μm generated more drizzle water content than was the case when $r_g = 0.05$ μm with no GCCN.

3) LES: $N = 150$ cm^{-3}, $r_g = 0.1$ μm

Due to the enormous computational expense of these simulations in 3D, only two runs are performed and for limited duration: one has no GCCN, and the other is seeded with 10^{-3} GCCN cm^{-3}. Comparisons are performed for the first 3 h of the simulation and shown in Fig. 9. First, comparing with the equivalent 2D simulation (Fig. 7) we see that the $w_{\rm rms}$ time series is much smoother in the 3D simulation but that the broad features of the development of turbulence are similar. LWP tends to be lower in the LES run. Second, comparing the LES runs over the last 80 min of the simulation, the inclusion of GCCN causes a depletion in LWP (6%) and in $w_{\rm rms}$ (10%). Surface R peaks at 0.2 mm d^{-1} after 3 h for the seeded case very close to the equivalent ERM simulation (cf. Fig. 7c). After 3 h, surface Z is also almost the same as in the ERM simulation (cf. Fig. 9d and Fig. 7d). In order to obtain some sense of how GCCN might affect results beyond the 3-h mark, the seeded simulation was continued to 4.5 h. In Fig. 9e, a comparison is made between I produced in the LES run with no GCCN (3-h simulation), the LES run with seeding (4.5-h simulation), and the equivalent ERM run (6-h simulation). The time series of I shows almost identical results up to the 4.5-h mark for the LES and ERM seeded cases, providing some level of confidence that the ERM results are representative of the more rigorous LES for this particular case study.

4. Discussion

a. Optical properties

1) TEM RESULTS

For the TEM results, the impact of GCCN is summarized in terms of the cloud susceptibility S defined as

$$S = \frac{A(1 - A)}{3N}, \tag{2}$$

(Twomey 1991) where albedo A has been approximated by

$$A \approx \frac{(1 - g)\tau}{2 + (1 - g)\tau} \tag{3}$$

(Bohren 1980), and g is the asymmetry factor (≈0.84). Cloud optical depth τ (in the visible) is given by

$$\tau \approx \int_{z_b}^{z_t} \int_0^\infty 2\pi r^2 n(r)\, dr\, dz, \tag{4}$$

where $n(r)$ defines the drop spectrum with respect to radius r, z_b is cloud base, z_t is cloud top, and the extinction efficiency has been assumed to be equal to 2. To simplify the discussion the standard definition of S for narrow monomodal drop spectra is used, rather than the modified form proposed by Feingold et al. (1997) for spectra undergoing collection broadening. Figure 10 summarizes TEM simulations with and without GCCN, for two median radii of CCN ($r_g = 0.1$ and $r_g = 0.05$ μm), as well as three different CCN concentrations (50, 150, and 250 cm^{-3}). Contrary to Fig. 6, S values for $r_g = 0.05$ μm are always larger than those for $r_g = 0.1$ μm regardless of whether GCCN are included at concentrations of 10^{-2} cm^{-3}. The percentage increase in S, due to GCCN or due to shifting the CCN median radius, is also qualitatively different from Fig. 6b: the maximum increase in S due to GCCN is now achieved in the midrange at $N_{\rm ccn} = 150$ cm^{-3} and is always greater for the smaller r_g. On the other hand, the decrease in r_g to 0.05 μm causes S to increase

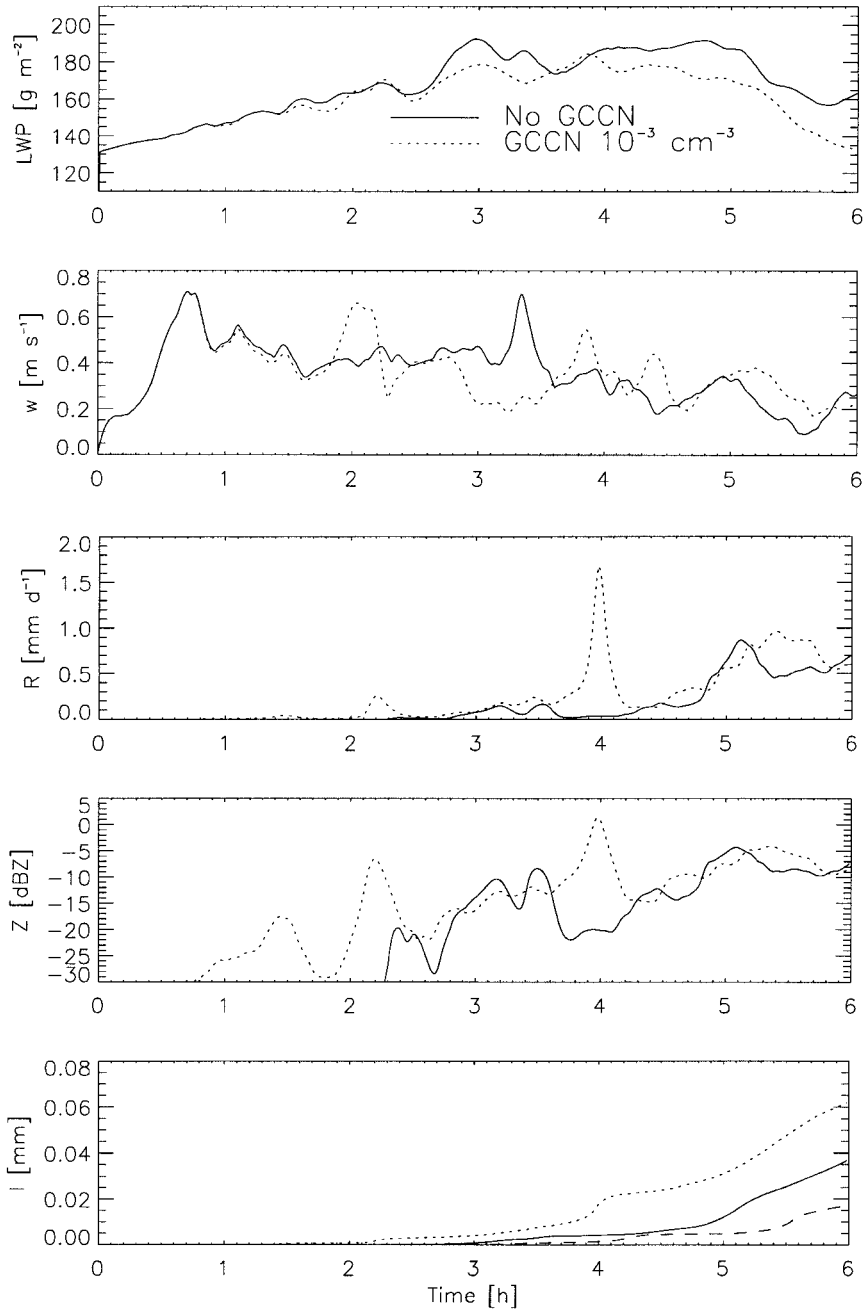

FIG. 8. As in Fig. 7, but for $N_{ccn} = 150$ cm^{-3} and $r_g = 0.05$ μm. In (e), the integrated surface precipitation I from Fig. 7 (no GCCN) has been included for comparison (dashed line).

monotonically with increasing N_{ccn} (for the situations simulated) and these increases are consistently larger than those incurred by GCCN.

Arguments applied to Fig. 6 for drizzle water r_d do not necessarily translate to S because τ (and therefore A) scales with r^2 whereas r_d scales with r^3. Also, the function $A(1 - A)$ is maximum at $A = 0.5$ so that the response of the system precludes simple conclusions.

2) ERM AND LES RESULTS

The temporal evolution of the ERM and LES results is displayed so that variations occurring as drizzle develops are captured. In the subsequent figures, six spatially and temporally averaged fields are displayed. The spatial averaging is over the cloudy domain and the temporal averaging is over the course of 1 h, beginning

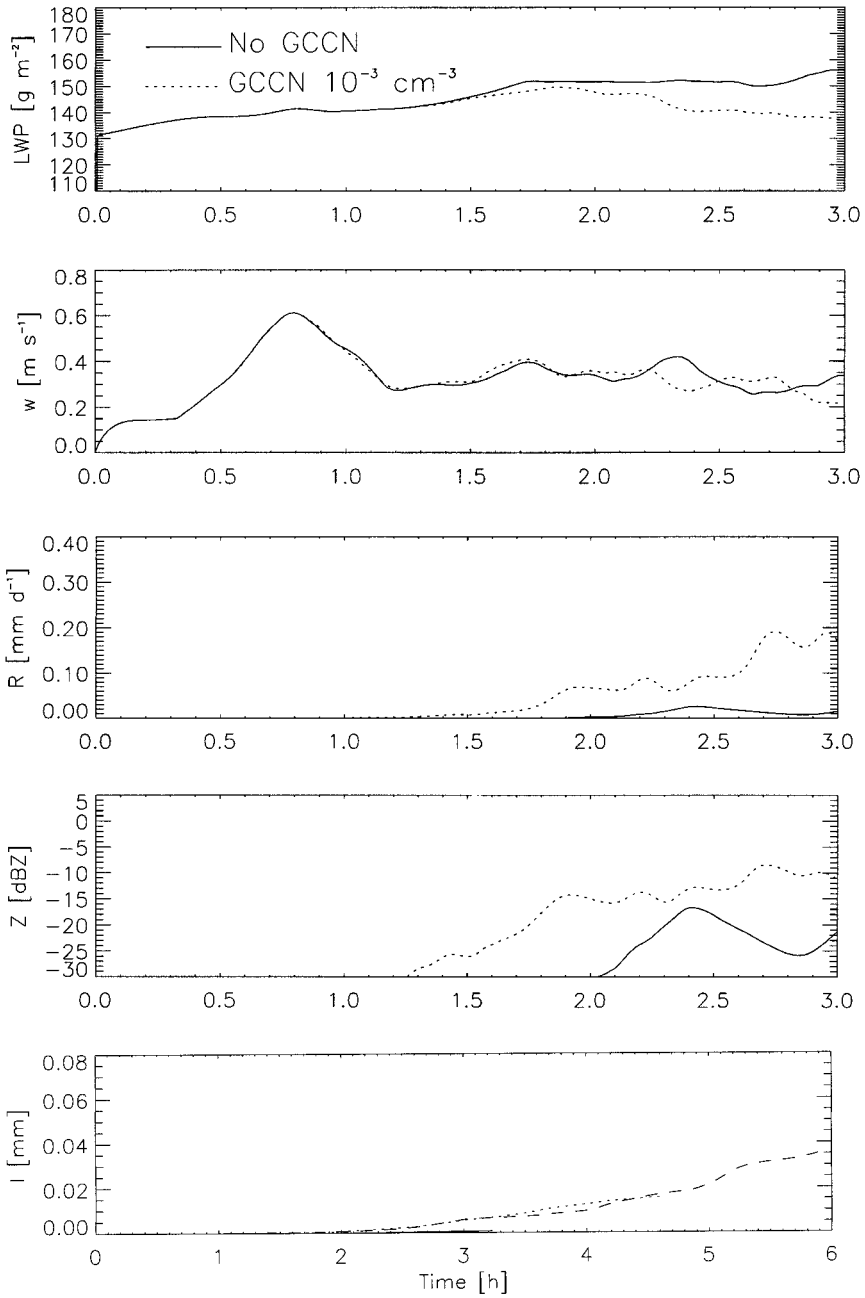

FIG. 9. As in Fig. 7, but for the LES simulation. In (e), the scale is changed from 3 to 6 h and *I* from Fig. 7 (ERM, no GCCN) is included for comparison (dashed line).

with the second hour. By averaging in this manner, we ignore cloud-scale inhomogeneities and focus on a comparison of these mean fields among the various cases. Figure 11 summarizes results pertaining to the ERM simulations in section 3 for $N_{ccn} = 150$ cm^{-3} and $r_g = 0.1$ μm. A progressive decrease in LWP, τ, N, and A, and an increase in r_e and S as a function of time relative to the runs without GCCN are noted. Most of the impact from the GCCN is achieved when GCCN are included at 10^{-3} cm^{-3}, which is consistent with Fig. 7. Figure 12 displays these same fields for the ERM simulations with $N_{ccn} = 150$ cm^{-3} and $r_g = 0.05$ μm. Evidence of the more active drizzle process is provided by strong depletion in LWP, τ, N, and A (more so than in Fig. 11), and concomitant increases in r_e and S. In a relative sense, the comparison between Figs. 11 and 12 supports the TEM results indicating that when the drizzle process is already quite active, the impact of GCCN at these

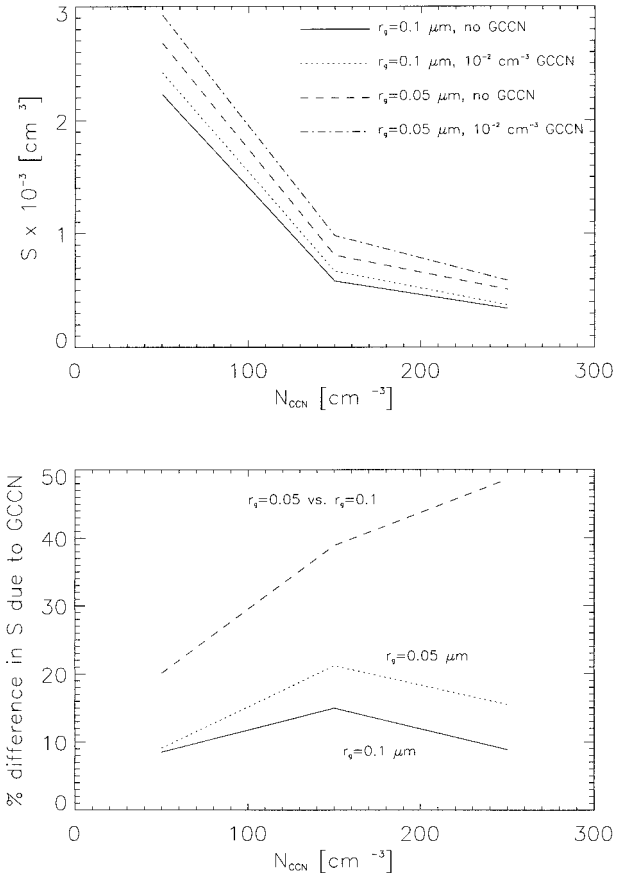

FIG. 10. (a) Calculations of TEM-derived values of susceptibility S as a function of N_{ccn} for various CCN spectra, and both with and without GCCN. (b) Percentage difference in S due to the addition of GCCN and due to the shift in r_g from 0.1 to 0.05 μm.

concentrations is diminished. Table 2 summarizes the 3-h average values of τ, A, and S for all ERM results—with and without GCCN. The percentage differences incurred in these parameters due to (i) the inclusion of GCCN and (ii) the shift in r_g appear in Table 3. We note that for τ and A, the impact of GCCN is of a similar order of magnitude to that of changing r_g; both effects cause a decrease of about 40% in τ and 20% in A. On the other hand, there is more variability in the impacts on S. The highest change in S (64%) results from decreasing r_g from 0.1 to 0.05 μm, whereas the lowest change in S comes from the inclusion of 10^{-3} cm^{-3} in the r_g = 0.05-μm case. The former is consistent with the TEM results in Fig. 10 whereas the latter is not; because different GCCN concentrations were used in each case it is unclear whether this is the cause of the difference, or whether the cause is the sedimentation process.

Finally, results for the first 3 h of the LES runs (Fig. 13, which can be compared with Fig. 11) show the same qualitative trends as those in the ERM and rather small quantitative differences, again providing confidence in the representativeness of the ERM results.

b. Balance between number and size of CCN

As shown in this work and that of many others, the number of droplets activated in a cloud and the subsequent evolution of the drop spectrum are ultimately a function of the size distribution (and composition) of CCN. The latter is controlled by sources and sinks of CCN in the BL (and to some extent, the free troposphere), as well as through cloud processing of the CCN spectrum. This occurs through a number of possible mechanisms, including homogeneous nucleation of new particles in regions of high relative humidity, aqueous chemistry, and drop collection. Hoppel et al. (1990) brought attention to the bimodal aerosol spectrum that is prevalent in the marine BL and argued that the mode of larger particles (approximately 0.1 μm) derives from particles that have undergone aqueous-chemistry processing. Bower and Choularton (1993) simulated SO_2 to sulfate conversion in an adiabatic parcel model and showed that in subsequent cloud cycles, this processing should enable more particles to be activated to droplets, and result in smaller r_e and more reflective clouds. In this scenario, clouds that process CCN would tend to become more reflective with time unless some means of breaking this cycle were available. One possible means is a source of GCCN that would induce collection before concentrations of droplets became too large. The concentration of CCN sufficient to affect the cloud would depend in general on the LWC of the cloud and the droplet concentration, as depicted in Fig. 1. Once active, the collection mechanism depletes the cloud drop concentration, and hence the number of CCN that can be regenerated by drops (e.g., Hudson 1993; Feingold et al. 1996b). If collection results in significant surface precipitation, even further reduction in N_{ccn} can be realized. If GCCN do not exist in high enough concentrations, then alternative mechanisms for producing small drizzle drops must be considered. One such mechanism is turbulent mixing (e.g., Baker et al. 1980). Another is through the size-differential effects of radiational cooling on condensational growth (e.g., Roach 1976; Harrington et al. 2000). Yet another, recently proposed by Zhang et al. (1999), is that aqueous chemistry might enhance drizzle drop formation. Using the TEM and a coupled cloud-microphysical–aqueous-chemistry model employing a moving mass grid, it was shown that aqueous chemistry processing of the CCN spectrum can enhance production of drops with r = 20 μm once sufficient cycling through cloud has occurred. If this hypothesis is verified by observation, it could indicate that although aqueous processing might increase drop concentrations, it could also produce sufficient numbers of small drizzle drops that could offset the tendency for N to increase. Ultimately a number of mechanisms might be acting simultaneously to broaden the droplet

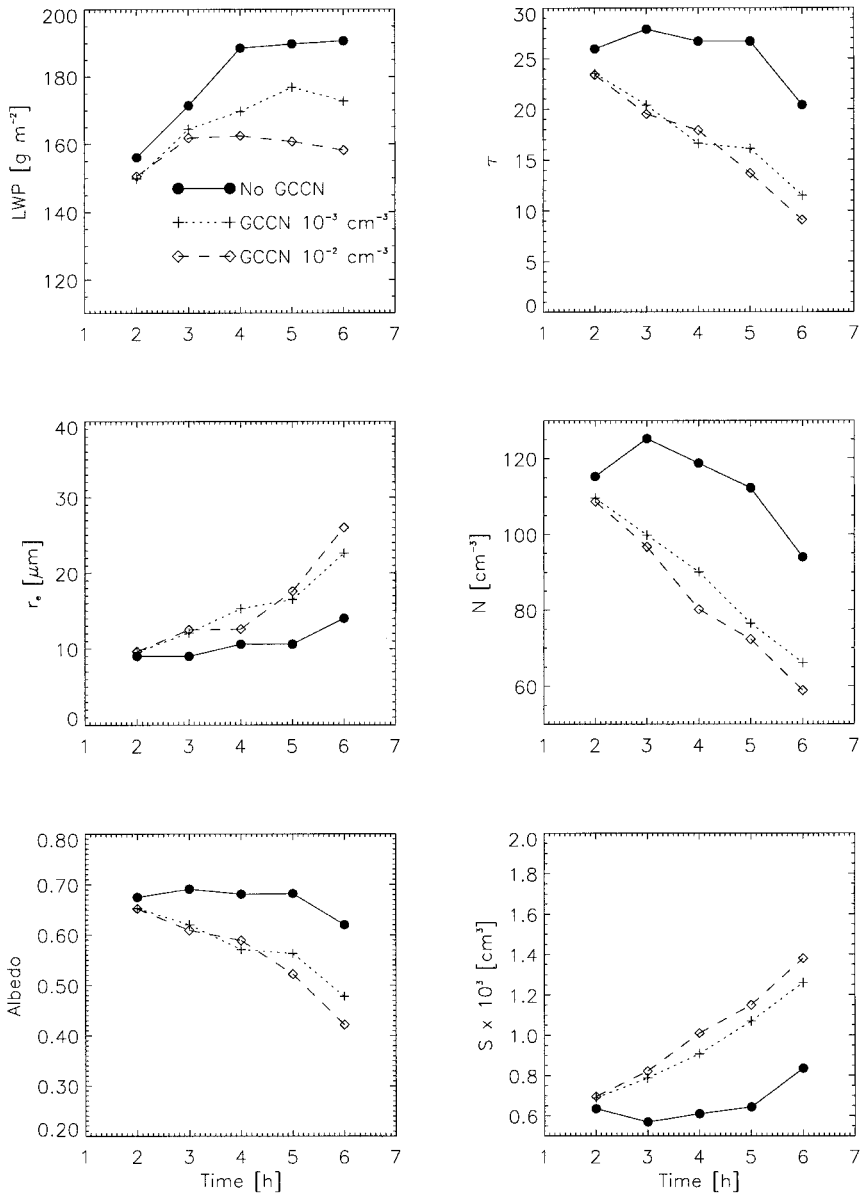

FIG. 11. ERM calculations of LWP, τ, effective radius r_e, N, A, and S for the course of a 6-h simulation. Data points represent averages over one hour. CCN are defined by $N_{ccn} = 150$ cm^{-3} and $r_g = 0.1$ μm.

spectrum; this work makes no attempt to evaluate their relative importance.

c. Ship wakes

During the recent Monterey Area Ship Track (MAST, June 1994) experiment, one of the hypotheses tested was that ship tracks result from sea-salt particles produced in the wake of a ship. Measurements indicated that particles produced in the wake of a ship are too few in number to produce ship tracks; this hypothesis was rejected in favor of the hypothesis that enhanced aerosol emissions from the ship's stack are the responsible agent. While the concentrations of *small* particles produced in the wake of a ship are undoubtedly too low to enhance cloud albedo, we raise the possibility that a counterhypothesis might be proposed, that is, that even very small concentrations of *giant* CCN may affect ship tracks by enhancing collection and therefore reducing the ship track albedo. Results in section 3 indicate that there are regions of N_{ccn}, r_l parameter space where GCCN may significantly enhance collection and decrease cloud albedo. Revisiting the MAST data with this in mind seems a worthwhile endeavor.

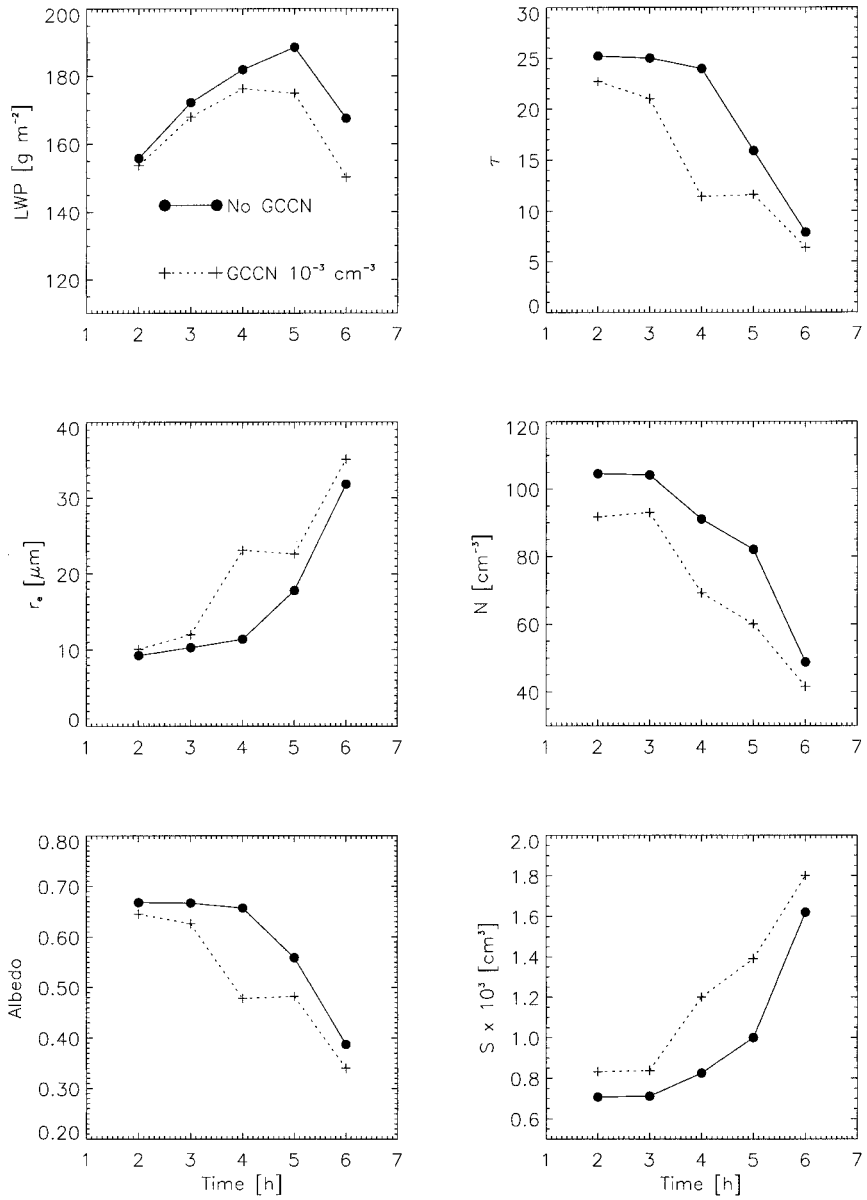

FIG. 12. As in Fig. 11 but for CCN defined by $N_{ccn} = 150$ cm^{-3} and $r_g = 0.05$ μm.

TABLE 2. Comparison of average values of τ, A, and S over the last 3 h of the ERM simulations for different CCN spectra, and both with and without GCCN.

	τ	A	S [$\times 10^{-3}$]
	$r_g = 0.1$ μm		
No GCCN	24.6	0.66	0.70
GCCN = 10^{-3} cm^{-3}	14.7	0.54	1.08
	$r_g = 0.05$ μm		
No GCCN	15.9	0.53	1.15
GCCN = 10^{-3} cm^{-3}	9.8	0.43	1.46

TABLE 3. Percentage difference in average values of τ, A, and S over the last 3 h of the ERM simulations due to 10^{-3} cm^{-3} GCCN (for $r_g = 0.1$ and $r_g = 0.05$ μm) and due to the shift in r_g.

	τ	A	S
Effect of GCCN:			
$r_g = 0.1$ μm	−40	−18	54
$r_g = 0.05$ μm	−38	−19	27
Effect of change in r_g	−35	−20	64

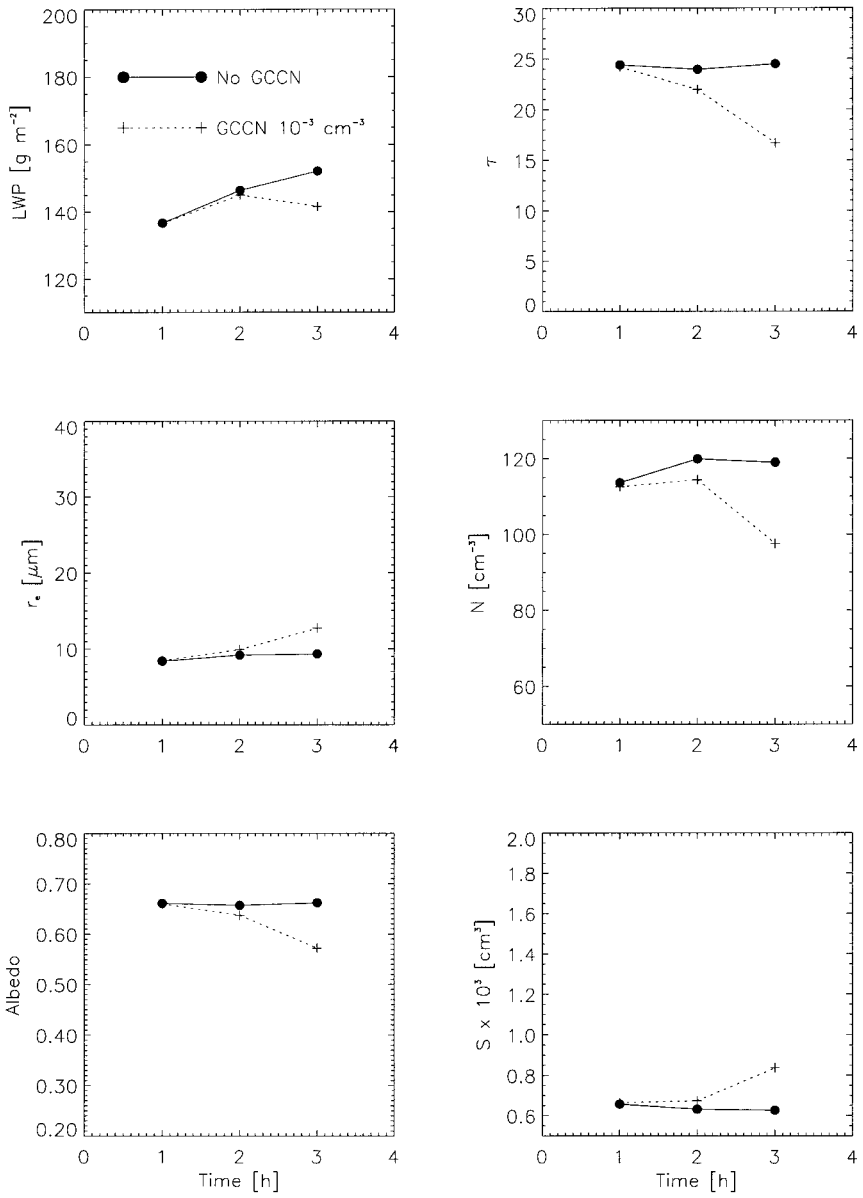

FIG. 13. As in Fig. 11 but for LES simulations of 3-h duration.

5. Summary and conclusions

This work has examined the impact of giant CCN on drizzle formation in stratocumulus clouds using a range of numerical models starting with a rather simple box model that simulates stochastic collection, through a trajectory ensemble model, and a 2D eddy-resolving model and a 3D large eddy simulation model. The goal has been to evaluate the impact of ambient GCCN concentrations on collection for parameter space that includes total CCN concentration or total drop concentration, LWC, and number concentration of GCCN.

Using the stochastic collection box model we have shown that GCCN affect collection over a rather narrow range of parameter space, but that the maximum *relative* effect occurs for N and LWC that vary in tandem, that is, large N and large LWC, or small N and small LWC (Fig. 1c). When LWC is high and N is low, drizzle is active anyway, and the addition of GCCN to the system has little impact. On the other hand, at low LWC and high N, the timescales for collection exceed those that can be realistically expected for parcel in-cloud residence times and, again, GCCN are of no consequence. These basic results also emerge from the other modeling frameworks and are quantified in various ways (e.g., Fig. 5 or Table 1 for the TEM; Figs. 7e, 8e, and 9e for the ERM and LES).

The TEM model is more representative of real clouds than the box model since it represents the spatial–tem-

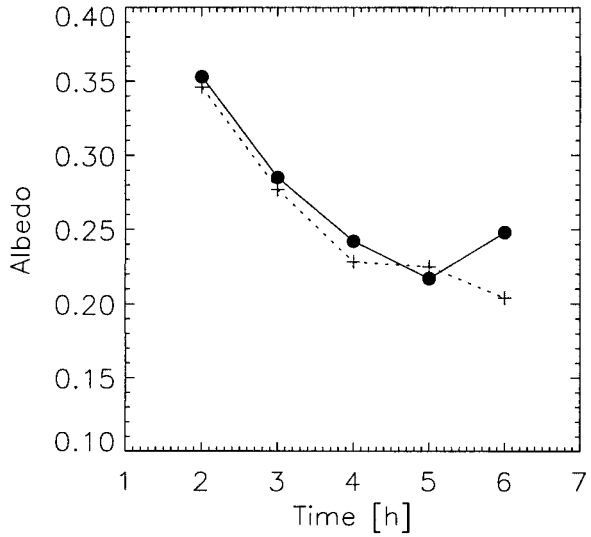

FIG. 14. Albedo calculation for an ERM simulation with the same initial conditions as in Fig. 11, except that $N_{ccn} = 50$ cm^{-3}.

poral changes in LWC that so strongly determine the rate of collection. Even brief sojourns into cloud under favorable conditions can have a significant impact on drizzle formation (Twomey 1976) and by considering an ensemble of parcels, these events can be represented. The TEM approach also has the salutary effect of enabling examination of the impact of collection on cloud optical properties that derive purely from microphysical effects, that is, without feedback to dynamics, and without drop sedimentation (one of the primary means by which microphysics feeds back to dynamics).

On the other hand, the ERM and LES (particularly the latter) represent our best attempt at integrating microphysical–dynamical interactions including precipitation. Summarizing the ERM and LES results for the cases examined in terms of integrated surface precipitation I, the following has been shown.

- The ERM results are consistent in nature and magnitude to the LES results for the limited overlap of cases examined.
- Measurable drizzle appears at the surface about 1 h earlier when GCCN exist in concentrations of 10^{-3} cm^{-3}. The -30 dBZ radar reflectivity associated with surface drizzle appears about 1.5 h earlier at this concentration of GCCN. After 6 h the addition of 10^{-3} cm^{-3} GCCN to a concentration of 150 cm^{-3} CCN enhances the integrated surface precipitation by 50% to 100%.
- For one case, the surface I after 6 h of simulation was not enhanced when GCCN were increased from 10^{-3} to 10^{-2} cm^{-3}. However, based on the TEM and box model results, it is expected that at higher CCN concentrations the extra GCCN would have an impact.
- A decrease in the median size of CCN from 0.1 to 0.05 μm enhanced I by about the same amount that 10^{-2} cm^{-3} GCCN did in the case of $r_g = 0.1$ μm.

Note that the TEM and ERM–LES results represent a single dynamical context pertaining to an ASTEX case study. Numerous experiments have been performed to investigate the effect of CCN and GCCN size and number concentrations on this system. Clearly caution must be exercised before extrapolating these results to other boundary layers which might exhibit different cloud water contents and/or parcel in-cloud residence times.

When examining the impact of GCCN on cloud optical properties such as S, τ, r_e and LWP, the ERM and LES results indicate a significant role for GCCN. For example, GCCN at concentrations of 10^{-3} cm^{-3} increase S by about 50% and decrease albedo by 23% after a 6-h simulation (Fig. 12). Note that in the scenario of CCN increases due to anthropogenic sources, the presence of GCCN must be considered. For example, examining Figs. 11 and 14 we see that if anthropogenic sources of CCN increase their concentration from 50 to 150 cm^{-3}, the albedo may increase from as low as 0.2 to over 0.6, or more than three-fold. Considering the presence of GCCN, however, moderates the effects of anthropogenic CCN considerably. If the altered air masses are in regions of strong sources of GCCN, say, where the boundary layer winds are strong, then increasing CCN concentrations from 50 to 150 cm^{-3} enhances cloud albedo only from 0.2 to about 0.4, or two-fold. Thus the variable presence of GCCN represents yet another uncertainty in estimating the influence of anthropogenic activity on climate.

Acknowledgments. Support for this work has been provided by NOAA (GF) as well as an NSF Grant ATM-9529321 entitled ''Simulations of cloud/radiative responses to variations in CCN'' (GF and WRC).

REFERENCES

Albrecht, B. A., C. S. Bretherton, D. Johnson, W. H. Schubert, and A. S. Frisch, 1995: The Atlantic Stratocumulus Transition Experiment-ASTEX. *Bull. Amer. Meteor. Soc.*, **76,** 889–904.

Baker, M. B., R. G. Corbin, and J. Latham, 1980: The influence of entrainment on the evolution of cloud droplet spectra: I. A model of inhomogeneous mixing. *Quart. J. Roy. Meteor. Soc.*, **106,** 581–598.

Blanchard, D. C., 1982: The production, distribution and bacterial enrichment of the sea salt aerosol. *Air–Sea Exchange of Gases and Particles,* P. S. Liss and W. G. N. Slinn, Eds., NATO ASI Series 108, 407–444.

Bohren, C. F., 1980: Multiple scattering of light and some of its observable consequences. *Amer. J. Phys.*, **55,** 524–533.

Bower, K. N., and T. W. Choularton, 1993: Cloud processing of the cloud condensation nucleus spectrum and its climatological consequences. *Quart. J. Roy. Meteor. Soc.*, **119,** 655–679.

Bretherton, C. S., P. Austin, and S. T. Siems, 1995: Cloudiness and marine boundary layer dynamics in the ASTEX Lagrangian experiments. Part II: Cloudiness, drizzle, surface fluxes, and entrainment. *J. Atmos. Sci.*, **52,** 2724–2735.

Cooper, W. A., R. T. Bruintjes, and G. K. Mather, 1997: Calculations

pertaining to hygroscopic seeding with flares. *J. Appl. Meteor.*, **36,** 1449–1469.

Duynkerke, P. G., H. Zhang, and P. J. Jonker, 1995: Microphysical and turbulent structure of nocturnal stratocumulus as observed during ASTEX. *J. Atmos. Sci.,* **52,** 2763–2777.

Exton, H. J., J. Latham, P. M. Park, M. H. Smith, and R. R. Allan, 1986: The production and dispersal of maritime aerosol. *Oceanic Whitecaps and Their Role in Air–Sea Exchange Processes,* E. C. Monahan and G. Mac Niocaill, Eds., Oceanic Sciences Library, D. Reidel, 175–193.

Feingold, G., B. Stevens, W. R. Cotton, and A. S. Frisch, 1996a: On the relationship between drop in-cloud residence time and drizzle production in stratocumulus clouds. *J. Atmos. Sci.,* **53,** 1108–1122.

——, S. M. Kreidenweis, B. Stevens, and W. R. Cotton, 1996b: Numerical simulation of stratocumulus processing of cloud condensation nuclei through collision–coalescence. *J. Geophys. Res.,* **101,** 21 391–21 402.

——, R. Boers, B. Stevens, and W. R. Cotton, 1997: A modeling study of the effect of drizzle on cloud optical depth and susceptibility. *J. Geophys. Res.,* **102,** 13 527–13 534.

——, S. M. Kreidenweis, and Y. Zhang, 1998: Stratocumulus processing of gases and cloud condensation nuclei. Part I: Trajectory ensemble model. *J. Geophys. Res.,* **103,** 19 527–19 542.

Hall, W. D., 1980: A detailed microphysical model within a two-dimensional dynamical framework: Model description and preliminary results. *J. Atmos. Sci.,* **37,** 2486–2507.

Harrington, J. Y., G. Feingold, W. R. Cotton, and S. M. Kreidenweis, 2000: Radiative impacts on the growth of a population of drops within simulated summertime arctic stratus. *J. Atmos. Sci.,* in press.

Hoppel, W. A., J. W. Fitzgerald, G. M. Frick, and R. E. Larson, 1990: Aerosol size distributions and optical properties found in the marine boundary layer over the Atlantic Ocean. *J. Geophys. Res.,* **95,** 3659–3686.

Houghton, H. G., 1938: Problems connected with the condensation and precipitation processes in the atmosphere. *Bull. Amer. Meteor. Soc.,* **19,** 152–159.

Hudson, J. G., 1993: Cloud condensation nuclei near marine cumulus. *J. Geophys. Res.,* **98,** 2693–2702.

Johnson, D. B., 1982: The role of giant and ultragiant aerosol particles in warm rain initiation. *J. Atmos. Sci.,* **39,** 448–460.

Khain, A. P., and M. B. Pinsky, 1995: Drop inertai amd its contribution to turbulent coalescence in convective clouds. Part I: Drop fall in the flow with random horizontal velocity. *J. Atmos. Sci.,* **52,** 196–206.

Kim, Y., H. Sievering, J. F. Boatman, D. Wellman, and A. A. P. Pszenny, 1995: Aerosol size distribution and aerosol water content measurements during the Azores Atlantic Stratocumulus Transition Experiment/Marine Aerosol and Gas Exchange experiment. *J. Geophys. Res.,* **100,** 23 027–23 038.

Klett, J. D., and M. H. Davis, 1973: Theoretical collision efficiencies of cloud droplets at small Reynolds numbers. *J. Atmos. Sci.,* **30,** 107–117.

Levin, Z., E. Ganor, and V. Gladstein, 1996: The effects of desert particles coated with sulfate on rain formation in the eastern Mediterranean. *J. Appl. Meteor.,* **35,** 1511–1523.

Mordy, W. A., 1959: Computations of the growth by condensation of a population of cloud droplets. *Tellus,* **11,** 16–44.

Paluch, I. R., and D. H. Lenschow, 1991: Stratiform cloud formation in the marine boundary layer. *J. Atmos. Sci.,* **48,** 2141–2158.

Roach, W. T., 1976: On the effect of radiative exchange on the growth by condensation of a cloud or fog droplet. *Quart. J. Roy. Meteor. Soc.,* **102,** 361–372.

Saffman, P. G., and J. S. Turner, 1956: On the collision of drops in turbulent clouds. *J. Fluid Mech.,* **1,** 16–30.

Stephens, G. L., 1978: Radiation profiles in extended water clouds. Part I: Theory. *J. Atmos. Sci.,* **35,** 2111–2122.

Stevens, B., G. Feingold, R. L. Walko, and W. R. Cotton, 1996: On elements of the microphysical structure of numerically simulated nonprecipitating stratocumulus. *J. Atmos. Sci.,* **53,** 980–1006.

——, W. R. Cotton, and G. Feingold, 1998a: A critique of one and two-dimensional models of marine boundary layer clouds with detailed representations of droplet microphysics. *Atmos. Res.,* **47–48,** 529–553.

——, ——, and ——, 1998b: Large-eddy simulations of strongly precipitating, shallow, stratocumulus-topped boundary layers. *J. Atmos. Sci.,* **55,** 3616–3638.

Twomey, S., 1976: The effects of fluctuations in liquid water content on the evolution of large drops by coalescence. *J. Atmos. Sci.,* **33,** 720–723.

——, 1991: Aerosols, clouds and radiation. *Atmos. Environ.,* **25A,** 2435–2442.

Tzivion, S., G. Feingold, and Z. Levin, 1987: An efficient numerical solution to the stochastic collection equation. *J. Atmos. Sci.,* **44,** 3139–3149.

——, T. Reisin, and Z. Levin, 1994: Numerical simulation of hygroscopic seeding in a convective cloud. *J. Appl. Meteor.,* **33,** 252–267.

Warren, S. G., C. J. Hahn, J. London, R. M. Chervine, and R. L. Jenne, 1986: Global distribution of total cloud cover and cloud type a mounts over ocean. NCAR Tech. Note. NCAR/TN-317+STR, 42 pp. [Available from NCAR, 1850 Table Mesa Dr., Boulder, CO 80307.]

Woodcock, A. H., 1953: Salt nuclei in marine air as a function of altitude and wind force. *J. Meteor.,* **10,** 362–371.

Wyant, M. C., C. S. Bretherton, H. Rand, and D. Stevens, 1997: Numerical simulations and conceptual model of the stratocumulus to trade cumulus transition. *J. Atmos. Sci.,* **54,** 168–192.

Zhang, Y., S. M. Kreidenweis, and G. Feingold, 1999: Stratocumulus processing of gases and cloud condensation nuclei. Part II: Chemistry sensitivity analysis. *J. Geophys. Res.,* **104,** 16 061–16 080.